



HAL
open science

Physical properties of the Hat aperiodic monotile: Graphene-like features, chirality and zero-modes

Justin Schirmann, Selma Franca, Felix Flicker, Adolfo G. Grushin

► To cite this version:

Justin Schirmann, Selma Franca, Felix Flicker, Adolfo G. Grushin. Physical properties of the Hat aperiodic monotile: Graphene-like features, chirality and zero-modes. 2023. hal-04242456

HAL Id: hal-04242456

<https://hal.science/hal-04242456>

Preprint submitted on 15 Oct 2023

HAL is a multi-disciplinary open access archive for the deposit and dissemination of scientific research documents, whether they are published or not. The documents may come from teaching and research institutions in France or abroad, or from public or private research centers.

L'archive ouverte pluridisciplinaire **HAL**, est destinée au dépôt et à la diffusion de documents scientifiques de niveau recherche, publiés ou non, émanant des établissements d'enseignement et de recherche français ou étrangers, des laboratoires publics ou privés.

Physical properties of the Hat aperiodic monotile: Graphene-like features, chirality and zero-modes

Justin Schirmann,^{1,*} Selma Franca ^{1,†} Felix Flicker ^{2,3,‡} and Adolfo G. Grushin ^{1,§}

¹*Univ. Grenoble Alpes, CNRS, Grenoble INP, Institut Néel, 38000 Grenoble, France*

²*School of Physics and Astronomy, Cardiff University,
The Parade, Cardiff CF24 3AA, United Kingdom*

³*School of Physics, H. H. Wills Physics Laboratory,
Tyndall Avenue, Bristol, BS8 1TL, United Kingdom*

(Dated: July 31, 2023)

The discovery of the Hat, an aperiodic monotile, has revealed novel mathematical aspects of aperiodic tilings. However, the physics of particles propagating in such a setting remains unexplored. In this work we study spectral and transport properties of a tight-binding model defined on the Hat. We find that (i) the spectral function displays striking similarities to that of graphene, including six-fold symmetry and Dirac-like features; (ii) unlike graphene, the monotile spectral function is chiral, differing for its two enantiomers; (iii) the spectrum has a macroscopic number of degenerate states at zero energy; (iv) when the magnetic flux per plaquette (ϕ) is half of the flux quantum, zero-modes are found localized around the reflected ‘anti-hats’; and (v) its Hofstadter spectrum is periodic in ϕ , unlike for other quasicrystals. Our work serves as a basis to study wave and electron propagation in possible experimental realizations of the Hat, which we suggest.

Introduction — Quasicrystals [1] exhibit a rich variety of physical properties beyond those observed in periodic crystals [2–4]. While long-range ordered like crystals, they lack periodicity, leading to novel electronic [5–10], optical [11–13], vibrational [2, 4], or topological phenomena [14–42]. Quasicrystalline materials derive their exotic behaviors from the symmetries of their quasilattices [43]. In two-dimensions (2D) quasilattice symmetries can often be described by aperiodic tilings of the plane [2, 4, 44–46].

Recently Smith *et al.* [47, 48] discovered the first example of a single, simply connected tile that tiles the plane only aperiodically. Dubbed ‘The Hat’, the shape admits a continuous range of deformations with the same property. The Hat’s structure factor is six-fold symmetric. As with other quasicrystals, the tiling can be understood as a slice through a higher-dimensional periodic lattice [49, 50]. The Hat quasilattice is chiral; it has two enantiomers related by mirror symmetry. The tiles are two mirrored images of the same tile (Fig. 1(a)): the hat, colored white, and the anti-hat, colored blue. A related tile, Tile(1,1), does not require its mirror image to tile the plane aperiodically [48].

Does the Hat imprint any novel physical properties on propagating particles compared to other two-dimensional aperiodic lattices? A fruitful strategy to answer this question is to define a vertex tight-binding model [5, 8, 16, 51] on the quasilattice, in which particles hop between nearest-neighbor vertices with equal probability. Vertex models have a single energy scale, the hopping, and hence conveniently isolate the effect of the graph connectivity on particle motion. They reveal unique spectral properties of quasicrystals, such as a multifractal spectrum [3, 8, 10, 16, 42, 52–55], characteristic of critical disorder systems [56], or exact zero-

modes [5, 8, 51, 57, 58]. Vertex models on 2D quasilattices differ from those of periodic 2D lattices by displaying an aperiodic Hofstadter spectrum as a function of an applied perpendicular magnetic flux per plaquette [14–17, 19, 21, 22, 40, 42].

In this work, we establish the spectral and transport properties of the Hat through its vertex tight-binding model. The momentum-resolved spectral function displays striking similarities with that of graphene, including putative Dirac cones and six-fold symmetry. However, unlike graphene, the Hat’s spectral function is chiral, and displays a predictable finite density of exact zero-modes. Lastly, as the Hat is a monotile, its Hofstadter spectrum is periodic in magnetic field flux, bypassing incommensurability effects of ‘polytiled’ quasicrystals [14–17, 19, 21, 22, 40]. The Hofstadter bands carry a Chern number that quantizes the two-terminal conductance in units of e^2/h . Hence, the physical properties of the Hat introduce a remarkable new class of phenomena between periodic crystals and aperiodic quasicrystals.

Spectral properties — The Hat quasilattice can be generated using ‘inflation rules’ in which four basic metatiles (combinations of hats), dubbed H, P, T and F, divide up into smaller versions of the same tiles, which are then inflated (rescaled) so all hats return to their original size [47]. Here, we define a tight-binding model on vertices of the second inflation of the H metatile, H2, shown in Fig. 1(a). Unless stated otherwise, our results apply to other tilings of the same hat tile. Each vertex is either two-, three- or four-fold coordinated, separated by three possible bond lengths. The average coordination number is $\langle z \rangle \sim 2.31$ and the average bond length is $\langle a \rangle = 1.37a_m$, with a_m the shortest bond length.

Setting all hoppings equal defines the vertex Hamilto-

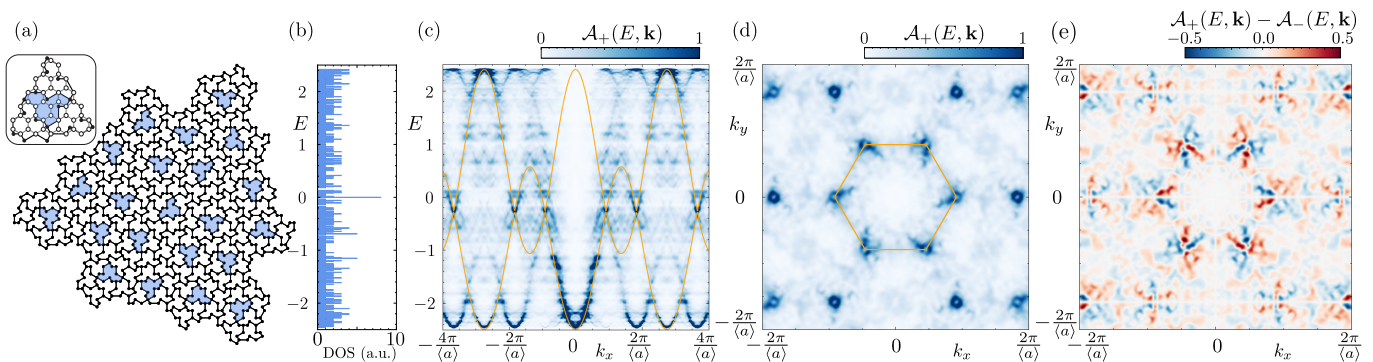


Figure 1. Spectral properties of the vertex model Eq. (1) on the Hat. (a) The H2 system with 22 anti-hats (reflected images of the hat tile) colored in blue. The inset shows a few hats of the system overlaid with a graphene approximant. (b) Density of states of the vertex model Eq. (1) on the H2 tiling. (c) Momentum-resolved spectral function $\mathcal{A}(E, \mathbf{k})$ (enantiomer $\mathcal{A}_+(E, \mathbf{k})$ in (e)) along the k_x momentum direction, calculated using the Kernel Polynomial method [59]. The dispersion relation for the lattice in (a) is overlaid in orange, with parameters $(a_g, t_1, t_2, \varepsilon_0) = (2a_m/\sqrt{3}, 0.82, -0.025, -0.2)$. (d) $\mathcal{A}(E, \mathbf{k})$ as a function of momentum $\mathbf{k} = (k_x, k_y)$ at $E = -0.2$. (e) The difference $\mathcal{A}_+(E, \mathbf{k}) - \mathcal{A}_-(E, \mathbf{k})$ between the spectral function $\mathcal{A}_+(E, \mathbf{k})$ of the system in (a) and the spectral function $\mathcal{A}_-(E, \mathbf{k})$ of its reflected image with respect to y -axis.

nian [5, 8, 51]

$$H_{\text{hat}} = -t \sum_{\langle ij \rangle} c_i^\dagger c_j + \text{h.c.} \quad (1)$$

The sum runs over all pairs of neighboring sites and the operators c_i^\dagger and c_i create and annihilate a particle on site i . We choose $t = 1$ without loss of generality.

The density of states (DOS) is shown in Fig. 1(b). As the tiling is non-bipartite the spectrum is not symmetric around zero energy [5]. The energy minimum $E_m \approx 2.4$ is well captured by the average coordination number $\langle z \rangle$ [5, 22]. Like other quasicrystals [10, 12], the Hat exhibits a fractal DOS with a multitude of van Hove singularities.

The probability of finding a state at energy E and momentum \mathbf{k} is determined by the spectral function, $\mathcal{A}(E, \mathbf{k}) = \langle \mathbf{k} | \delta(H_{\text{hat}} - E) | \mathbf{k} \rangle$, shown in Fig. 1(c) and (d) for H2. This function is well defined even without translational invariance [60–66] as it measures the overlap of the eigenstates with plane-waves of well-defined momentum \mathbf{k} , $\langle \mathbf{r} | \mathbf{k} \rangle = \frac{1}{\sqrt{N}} e^{i\mathbf{k} \cdot \mathbf{r}}$, with $\iota^2 = -1$, N the number of vertices and $\mathbf{r} = (x, y)$ their positions. The spectral function has been measured using angle-resolved photoemission experiments in quasicrystals [64–66].

The spectral function shows, close to zero energy, Dirac node-like features reminiscent of graphene’s band structure. To quantify this similarity we define a periodic hexagonal lattice that we call the graphene approximant. The graphene lattice constant $a_g = 2a_m/\sqrt{3}$ is chosen such that the associated honeycomb lattice (inset of Fig. 1(a)) captures many ($\approx 53\%$) of the Hat’s vertices. The graphene approximant’s dispersion and periodicity capture several features of $\mathcal{A}(E, \mathbf{k})$ (orange lines in Figs. 1(c), (d)). The approximant’s dispersion relation is [67]

$$E_{\pm}(\mathbf{k}) = \pm t_1 \sqrt{3 + f(\mathbf{k})} - t_2 f(\mathbf{k}) + \varepsilon_0, \quad (2)$$

where $f(\mathbf{k}) = 2 \cos(\sqrt{3}k_x) + 4 \cos(\sqrt{3}k_x/2) \cos(3k_y/2)$, t_1 and t_2 are first and second nearest-neighbor hopping amplitudes and ε_0 is the energy offset. Here, we use $(a_g, t_1, t_2, \varepsilon_0) = (2a_m/\sqrt{3}, 0.82, -0.025, -0.2)$. A nonzero t_2 and ε_0 mimic the Hat spectrum’s asymmetry. The approximant’s Brillouin zone is represented with orange lines in Fig. 1(d). The zone corners match the location of the Dirac node-like features close to $E = -0.2$. The Hat’s C_6 symmetry [49] is apparent in Fig. 1(d). This analysis confirms a quantitative similarity between the spectral properties of graphene and the Hat, rooted in the large number of vertices they share.

Unlike graphene, we can define an enantiomer of the Hat lattice by applying a reflection operator. The difference between the two corresponding enantiomorphic spectral functions $\mathcal{A}_+(\omega, \mathbf{k}) - \mathcal{A}_-(\omega, \mathbf{k})$ reveals that chiral properties are spread across the quasi-Brillouin zone (Fig. 1(e)).

Zero-energy states — Another striking feature dissimilar to graphene is the existence of a finite density of zero-energy states (Fig. 2(a)). We observe that the number of zero-modes can increase or decrease upon adding tiles (see the Supplemental Material (SM) [69] for some simple examples). Similar zero-modes have been found in numerous quasilattices, including the Penrose tiling [5, 57, 70, 71], the Ammann-Beenker tiling [58, 72, 73], and quasicrystalline graphene bilayers [74].

In Fig. 2(b) we plot the local density of states (LDOS) at zero energy corresponding to H2, Fig. 1(a). While some of the zero-mode weight can be explained as arising from zero-modes of each underlying metal of the previous generation (colored areas in Fig. 2(b)), we observe that the finite weight on T1 within H2, Fig. 2(b), is absent in a standalone T1 quasicrystallite shown in Fig. 2(c).

However, all of our zero-modes can be understood in

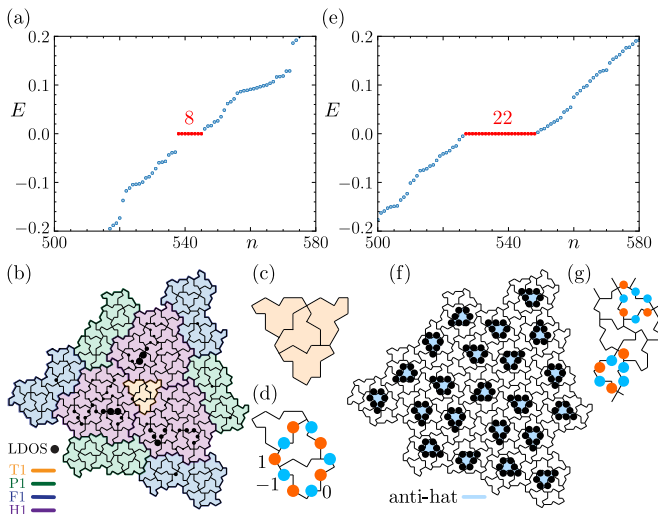


Figure 2. Zero-modes under 0- and π -flux. (a) Low-energy spectrum of the Hat lattice without flux. The eight exact zero-modes are colored in red. (b) The associated local density of states (LDOS) of these zero-modes. Colors highlight previous inflation generations composing the H2 quasilattice: T1, P1, F1 and H1. (c) The T1 quasicrystallite has no zero-modes. (d) The T1 quasicrystallite without the rightmost hat, has a single zero-mode. The overlaid zero-mode amplitudes form the Sutherland loop sequence $\{0, 1, 0, -1\}^m$ [68] of length $4m$, with $m \in \mathbb{Z}$. (e) The low-energy spectrum of the Hat system under π -flux. The 22 exact zero-modes are colored in red. (f) Corresponding zero-energy LDOS, pinned to anti-hats. (g) A zoom-in of the wave-function corresponding to the eigenstate 530. Because $\phi/\phi_0 = 1/2$, the Sutherland loop is modified to have one defect per anti-hat.

terms of the graph connectivity. The tight-binding model defines the adjacency matrix of the corresponding undirected graph; the zero-modes then form an orthogonal basis for its null space. A basis can always be found in which each (un-normalized) zero-mode has integer amplitudes on all vertices (see SM [69] for proof). As in the Ammann-Beenker tiling, these modes are fragile in the sense that they rely on equal hoppings to remain at strictly zero energy [71, 73].

For a nearest-neighbor vertex model, like Eq. (1), the zero energy condition implies that for every site i , the sum of the amplitudes on all neighbors j of i must vanish: $\sum_j \Psi_j = 0$ [68]. In the SM [69] we prove that whenever all hoppings are rational (equal to one here), all energy eigenstates corresponding to integer energies (equal to zero here) can be chosen to have integer amplitudes on all vertices, before normalization. In the Hat tiling the simplest zero-modes take the form of cycles of length $4m$, with m integer. Here the amplitudes around the cycle can be taken to be the repeated sequence $\{0, 1, 0, -1\}^m$ whenever vertices from the rest of the graph connect only to cycle vertices of zero amplitude or connect to pairs of vertices with opposite amplitude. This form is a generalization of one identified by Sutherland [5, 68]; we term

it a Sutherland loop.

In Figs. 2(c) and (d) we show two quasicrystallites that differ by one hat. Diagonalizing, we find no zero-modes in (c) and one zero-mode in (d). Removing the extra hat allows for a 20-vertex Sutherland loop shown in Fig. 2(d). Larger quasicrystallites contain integer-amplitude zero-modes not of the Sutherland loop form. In general, all integer-amplitude zero-modes of a given quasicrystallite can be exactly enumerated by finding the *Hermite normal form* of the adjacency matrix (see SM [69]) [75, 76].

π -flux zero-modes — The shortest loops, which circle around a single tile, cannot be Sutherland loops as they have a length of 13 or 14. However, anti-hats, the enantiomorphic minority tiles which have two four-fold coordinated sites (blue hats in Fig. 1(a)), can support a zero-mode if we allow a sign flip of one of the hoppings around the anti-hat. This is equivalent to threading a magnetic flux of π per anti-hat, as the electron wavefunction picks up a minus sign as it goes around due to the Aharonov-Bohm effect. As all the hats and anti-hats have the same area, this suggests that applying a perpendicular magnetic field with exactly π -flux per plaquette should generate one zero-mode per anti-hat. In fact, we find that these are the only zero-modes in this setting.

To model a perpendicular magnetic field B we introduce a Peierls phase by changing the hopping from site j to site i as $t \rightarrow t \exp(-i\pi \frac{\phi}{\phi_0} (x_i - x_j)(y_i + y_j)/\mathcal{A})$, where $\mathcal{A} = 8\sqrt{3}a_m^2$ is the hat area and $\phi_0 = h/e$ is the magnetic flux quantum. When $\phi/\phi_0 = 1/2$ the hoppings can be chosen to be real, with every hat tile having an odd number of negative bonds compared to Eq. (1). The spectrum close to $E = 0$ is shown in Fig. 2(e). For all systems inflated from primitive metatiles H0, T0, P0 and F0 that we have checked, we observe that the number of zero-modes equals the number of anti-hats (see SM [69]). Their LDOS is localized exactly at the anti-hats, as exemplified by Fig. 2(f). Because $\phi/\phi_0 = 1/2$, the wavefunction amplitude has exactly one defect per anti-hat, compared to the Sutherland loop sequence, as shown in Fig. 2(g).

Hofstadter spectrum — In Fig. 3(a) we show the bulk spectrum of H3, the third inflation of the H metatile, as a function of ϕ/ϕ_0 . To isolate the bulk spectrum we exclude states whose weight inside the yellow line in Fig. 3(b) is smaller than their weight outside it.

With our normalization, the spectrum is periodic in the interval $\phi/\phi_0 \in [0, 1)$. This is a special feature of monotiles, compared to other quasicrystals: as there is only one type of plaquette there is only one area \mathcal{A} to normalize the flux, and hence the spectrum is periodic. A typical quasicrystal spectrum is aperiodic as a function of ϕ/ϕ_0 [15, 32, 40, 77], unless one considers commensurate quasicrystals composed of tiles with commensurate areas [21, 22].

When the magnetic length $l_B \ll a_m$, the spectrum

splits into Landau levels near the bottom of the spectrum ($E \sim -2.4$), and disperses linearly with B [22]. In the Hofstadter regime $l_B \gg a_m$, the spectrum is split into Hofstadter bands separated by gaps. If the Fermi energy E_F is placed within these gaps, we expect the system to display topological edge states and a quantized Hall conductance [78, 79].

The topological properties of aperiodic 2D systems without time-reversal symmetry are captured by a quantized bulk average \mathcal{C} of the local Chern marker \mathcal{C}_r [80]. Mathematically, $\mathcal{C} = \frac{1}{\mathcal{A}_b} \sum_{\mathbf{r} \in \mathcal{A}_b} \mathcal{C}_r$, with \mathcal{A}_b the area of a bulk region highlighted in Fig. 3(b), $\mathcal{C}_r = \langle \mathbf{r} | \hat{C} | \mathbf{r} \rangle$ and

$$\hat{C} = 2\pi i \left(\hat{P} \hat{X} \hat{Q} \hat{Y} \hat{P} - \hat{P} \hat{Y} \hat{Q} \hat{X} \hat{P} \right). \quad (3)$$

Here $\hat{P} = \sum_{E < E_F} |\Psi\rangle \langle \Psi|$ is the projector onto occupied states, $\hat{Q} = 1 - \hat{P}$, and \hat{X} and \hat{Y} are position operators. In a topological phase $\mathcal{C} \in \mathbb{Z}$ and coincides with the Chern number for periodic systems [80].

Fig. 3(b) shows \mathcal{C}_r for $E_F = -1.58$ and $\phi/\phi_0 = 0.2$; $\mathcal{C} \approx -1$ in the bulk, as expected for a topologically non-trivial phase [80]. The bulk value of \mathcal{C} in the interval $\phi/\phi_0 \in [0, 1/2]$ is shown in Fig. 3(c). Regions with non-trivial Chern numbers match the positions of bulk gaps in Fig. 3(a), confirming the presence of topological edge states.

The physical imprint of topological edge states is a quantized two-terminal conductance G , in units of $G_0 = e^2/h$. To confirm this, we attach two leads to two boundary regions of H3, see Fig. 3(b). These leads consist of decoupled waveguides of dispersion $-2 \cos k_z$, oriented along the z -direction and placed such that each waveguide probes a single site of the Hat quasilattice. The two-terminal conductance G is then defined in the Landauer-Buttiker formalism [81] as $G = G_0 \text{Tr}[\tau \tau^\dagger]$, where $G_0 = e^2/h$ is the conductance quantum and τ is the transmission matrix between two leads calculated using the KWANT package [82].

The conductance map as a function of ϕ/ϕ_0 and E is shown in Fig. 3(d). In regions with non-zero density of bulk states, the conductance exhibits fluctuations observed in topologically trivial quasicrystals [3]. However, inside the bulk gaps with nontrivial $\mathcal{C} = \pm 1$, $G = G_0$, stemming from a topological boundary state. Finite size effects are visible in smaller gaps with larger \mathcal{C} , see Fig. 3(c), where G deviates from quantization.

Physical properties of Tile(1,1) — To conclude, we comment on the physical properties of a vertex model of Tile(1,1) [47, 48]. With a geometric modification, Tile(1,1) tiles the plane only aperiodically without its mirror image. This modified form is called ‘the Spectre’; since we are interested only in graph connectivity we use the names Tile(1,1) and Spectre interchangeably. Tile(1,1) contains special tiles similar to the anti-hats. Here they appear $\pi/6$ rotated from the other tiles, which

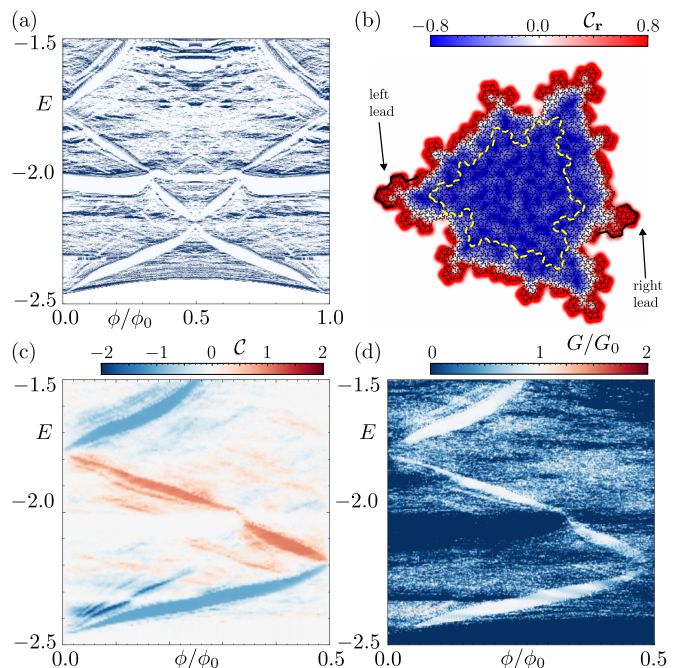


Figure 3. Hofstadter spectrum and quantized conductance. (a) The bulk Hofstadter spectrum Eq. (1) calculated for the H3 quasilattice near the band bottom. (b) The local Chern marker \mathcal{C}_r calculated for the H3 quasilattice (black) at $E = -1.58$ and $\phi/\phi_0 = 0.2$, i.e. for a state located inside the bulk gap of panel (a). The yellow dashed line delimits the bulk area \mathcal{A}_b used to produce panels (a) and (c). Inside \mathcal{A}_b , the marker averages to $\mathcal{C} = -1.03$. Thick black lines on the edges denote sites where leads are attached. (c) \mathcal{C} as a function of E and ϕ/ϕ_0 . Bulk gap regions of panel (a) have nontrivial Chern numbers. (d) Corresponding two-terminal conductance map. Where $|\mathcal{C}| = 1$, the conductance is quantized to $G = G_0 = e^2/h$, confirming the role of topological boundary modes in transport.

appear only $\pi/3$ rotated from one another. As with the anti-hats, these tiles always have two four-fold coordinated vertices. We term them anti-spectres. As Tile(1,1) is a member of the continuous family of tiles connected to the Hat it is pertinent to ask which properties it maintains.

Unlike the Hat, the vertices of Tile(1,1) do not fit to a periodic hexagonal lattice. The graphene-like features are therefore washed out. However, the quasilattice remains chiral, so it remains true that $\mathcal{A}_+(\omega, \mathbf{k}) - \mathcal{A}_-(\omega, \mathbf{k}) \neq 0$. Tile(1,1) also displays strictly localized zero-modes that have a similar origin to those in the Hat. In the presence of a π -flux, each anti-spectre again localizes a zero-mode. In all the cases we have checked, these again exhaust all zero-modes. The Hofstadter spectrum is again periodic (as the Spectre is a monotile), and displays topological gaps with quantized conductance.

Conclusions — Particles hopping on the Hat and Spectre monotiles present physical properties that set them aside from previously known 2D crystals and qua-

sicrystals. The Hat displays graphene-like features in its spectral function, notably putative Dirac cones and six-fold symmetry. Their origin is intrinsic, different from quasicrystalline graphene bilayers [39, 83, 84] that inherit these features from the underlying graphene layers. In the Hat, the intrinsic Dirac-cone-like features resemble those found in graphene in the presence of a small density of topological defects [85].

In the near term, a vertex model of the tiling may be realized in metamaterials, where complex phases mimicking magnetic fields can be engineered [86]. Quasicrystals have been realized in photonic metamaterials [18, 86–88], polaritonic systems [89], electrical circuits [90], microwave networks [91], and acoustic [92] and mechanical [93] metamaterials.

While no material has yet been discovered with the symmetries of the Hat it would seem likely that nature would realize such an elegant construction, just as Penrose tilings were discovered to describe the surfaces of icosahedral quasicrystals [94–97]. A promising solid-state platform is the engineered adsorption of atoms to constrain scattering of surface states. CO molecules on metals have been used to construct artificial honeycomb [98] and fractal [99] lattices. 2D lattices of Shiba states caused by magnetic ad-atoms on superconductors serve to engineer topological phases [100–102].

Chiral crystals display richer physical responses than achiral crystals [103]. The Hat tiling should share some of these features with their chiral crystalline counterparts, including magnetochiral anisotropy [104] and optical gyrotropy [105–108]. Additionally, adding defects or particle interactions to vertex-monotile models can generalize other works on interacting quasicrystals [32, 72, 109, 110]. We leave the study of these effects for subsequent work.

Acknowledgements We thank E. König for illuminating discussions. We also thank the authors of Refs. 47 and 48, especially Craig Kaplan for publishing their programs to generate Hat tilings [111]. A.G.G. and S. F. acknowledge financial support from the European Union Horizon 2020 research and innovation program under grant agreement No. 829044 (SCHINES). J. S. is supported by the program QuantEdu-France n° ANR-22-CMAS-0001 France 2030. F.F. was supported by EPSRC grant EP/X012239/1. A. G. G. is also supported by the European Research Council (ERC) Consolidator grant under grant agreement No. 101042707 (TOPOMORPH). This research was supported in part by the National Science Foundation under Grant No. NSF PHY-1748958.

* justin.schirmann@neel.cnrs.fr;

* These two authors contributed equally

† selma.franca@neel.cnrs.fr;

† These two authors contributed equally

‡ flicker@cardiff.ac.uk

§ adolfo.grushin@neel.cnrs.fr




- [1] D. Shechtman, I. Blech, D. Gratias, and J. W. Cahn, Metallic Phase with Long-Range Orientational Order and No Translational Symmetry, *Phys. Rev. Lett.* **53**, 1951 (1984).
- [2] C. Janot, *Quasicrystals - A Primer* (Clarendon Press Oxford, 1992).
- [3] Z. Stadnik, *Physical Properties of Quasicrystals* (Springer Series in Solid-State Sciences, 1999).
- [4] T. Janssen, G. Chapuis, and M. d. Boissieu, *Aperiodic Crystals From Modulated Phases to Quasicrystals*, Acta Crystallographica Section A, Vol. 74 (Oxford University Press, 2018).
- [5] M. Kohmoto and B. Sutherland, Electronic states on a Penrose lattice, *Phys. Rev. Lett.* **56**, 2740 (1986).
- [6] J. P. Lu and J. L. Birman, Electronic structure of a quasiperiodic system, *Phys. Rev. B* **36**, 4471 (1987).
- [7] A. P. Smith and N. W. Ashcroft, Pseudopotentials and quasicrystals, *Phys. Rev. Lett.* **59**, 1365 (1987).
- [8] T. Fujiwara, M. Arai, T. Tokihiro, and M. Kohmoto, Localized states and self-similar states of electrons on a two-dimensional Penrose lattice, *Phys. Rev. B* **37**, 2797 (1988).
- [9] H. Tsunetsugu, Conductance fluctuation of a Penrose tiling, *Journal of Non-Crystalline Solids* **117**, 781 (1990).
- [10] T. Rieth and M. Schreiber, Numerical investigation of electronic wave functions in quasiperiodic lattices, *Journal of Physics: Condensed Matter* **10**, 783 (1998).
- [11] D. Mayou, Generalized Drude formula for the optical conductivity of quasicrystals, *Phys. Rev. Lett.* **85**, 1290 (2000).
- [12] S. Burkov and S. Rashkeev, On optical properties of quasicrystals and approximants, *Solid State Communications* **92**, 525 (1994).
- [13] T. Timusk, J. P. Carbotte, C. C. Homes, D. N. Basov, and S. G. Sharapov, Three-dimensional Dirac fermions in quasicrystals as seen via optical conductivity, *Phys. Rev. B* **87**, 235121 (2013).
- [14] M. Arai, T. Tokihiro, and T. Fujiwara, Electronic structure of a 2D Penrose lattice in a magnetic field, *Journal of the Physical Society of Japan* **56**, 1642 (1987).
- [15] T. Hatakeyama and H. Kamimura, Fractal nature of the electronic structure of a Penrose tiling lattice in a magnetic field, *Journal of the Physical Society of Japan* **58**, 260 (1989).
- [16] F. Piéchon and A. Jagannathan, Energy-level statistics of electrons in a two-dimensional quasicrystal, *Phys. Rev. B* **51**, 179 (1995).
- [17] J. Vidal and R. Mosseri, Quasiperiodic tilings in a magnetic field, *Journal of Non-Crystalline Solids* **334**, 130 (2004).
- [18] Y. E. Kraus, Y. Lahini, Z. Ringel, M. Verbin, and O. Zeitlinger, Topological States and Adiabatic Pumping in Quasicrystals, *Phys. Rev. Lett.* **109**, 106402 (2012).
- [19] D. T. Tran, A. Dauphin, N. Goldman, and P. Gaspard, Topological Hofstadter insulators in a two-dimensional quasicrystal, *Phys. Rev. B* **91**, 085125 (2015).
- [20] I. C. Fulga, D. I. Pikulin, and T. A. Loring, Aperiodic Weak Topological Superconductors, *Phys. Rev. Lett.* **116**, 257002 (2016).
- [21] J.-N. Fuchs and J. Vidal, Hofstadter butterfly of a quasicrystal, *Phys. Rev. B* **94**, 205437 (2016).

- [22] J.-N. Fuchs, R. Mosseri, and J. Vidal, Landau levels in quasicrystals, *Phys. Rev. B* **98**, 145 (2018).
- [23] H. Huang and F. Liu, Theory of spin Bott index for quantum spin Hall states in nonperiodic systems, *Phys. Rev. B* **98**, 125130 (2018).
- [24] H. Huang and F. Liu, Quantum spin Hall effect and spin Bott index in a quasicrystal lattice, *Phys. Rev. Lett.* **121**, 126401 (2018).
- [25] A.-L. He, L.-R. Ding, Y. Zhou, Y.-F. Wang, and C.-D. Gong, Quasicrystalline Chern insulators, *Phys. Rev. B* **100**, 214109 (2019).
- [26] T. A. Loring, Bulk spectrum and K-theory for infinite-area topological quasicrystals, *Journal of Mathematical Physics* **60**, 081903 (2019).
- [27] R. Chen, D.-H. Xu, and B. Zhou, Topological Anderson insulator phase in a quasicrystal lattice, *Phys. Rev. B* **100**, 115311 (2019).
- [28] D. Varjas, A. Lau, K. Pöyhönen, A. R. Akhmerov, D. I. Pikulin, and I. C. Fulga, Topological Phases without Crystalline Counterparts, *Phys. Rev. Lett.* **123**, 196401 (2019).
- [29] H. Huang, Y.-S. Wu, and F. Liu, Aperiodic topological crystalline insulators, *Phys. Rev. B* **101**, 145 (2020).
- [30] C.-B. Hua, R. Chen, B. Zhou, and D.-H. Xu, Higher-order topological insulator in a dodecagonal quasicrystal, *Phys. Rev. B* **102**, 241102 (2020).
- [31] J. D. Cain, A. Azizi, M. Conrad, S. M. Griffin, and A. Zettl, Layer-dependent topological phase in a two-dimensional quasicrystal and approximant, *Proceedings of the National Academy of Sciences* **117**, 26135 (2020).
- [32] C. W. Duncan, S. Manna, and A. E. B. Nielsen, Topological models in rotationally symmetric quasicrystals, *Phys. Rev. B* **101**, 115413 (2020).
- [33] O. Zilberberg, Topology in quasicrystals, *Opt. Mater. Express* **11**, 1143 (2021).
- [34] D. V. Else, S.-J. Huang, A. Prem, and A. Gromov, Quantum many-body topology of quasicrystals, *Phys. Rev. X* **11**, 041051 (2021).
- [35] J. Fan and H. Huang, Topological states in quasicrystals, *Frontiers of Physics* **17**, 13203 (2021).
- [36] C.-B. Hua, Z.-R. Liu, T. Peng, R. Chen, D.-H. Xu, and B. Zhou, Disorder-induced chiral and helical Majorana edge modes in a two-dimensional Ammann-Beenker quasicrystal, *Phys. Rev. B* **104**, 155304 (2021).
- [37] R. Ghadimi, T. Sugimoto, K. Tanaka, and T. Tohyama, Topological superconductivity in quasicrystals, *Phys. Rev. B* **104**, 144511 (2021).
- [38] T. Peng, C.-B. Hua, R. Chen, Z.-R. Liu, D.-H. Xu, and B. Zhou, Higher-order topological Anderson insulators in quasicrystals, *Phys. Rev. B* **104**, 245302 (2021).
- [39] A. Shi, Y. Peng, J. Jiang, Y. Peng, P. Peng, J. Chen, H. Chen, S. Wen, X. Lin, F. Gao, and J. Liu, Unconventional higher-order topology in quasicrystals, *Preprint at <https://arxiv.org/abs/2209.05751>* (2022).
- [40] D. Johnstone, M. J. Colbrook, A. E. B. Nielsen, P. Öhberg, and C. W. Duncan, Bulk localized transport states in infinite and finite quasicrystals via magnetic aperiodicity, *Phys. Rev. B* **106**, 045149 (2022).
- [41] C. Wang, F. Liu, and H. Huang, Effective model for fractional topological corner modes in quasicrystals, *Phys. Rev. Lett.* **129**, 056403 (2022).
- [42] J. Jeon, M. J. Park, and S. Lee, Length scale formation in the Landau levels of quasicrystals, *Phys. Rev. B* **105**, 045146 (2022).
- [43] Quasilattices are sets of delta functions with the symmetries of the physical quasicrystals, in exact analogy to the relationship between crystal lattices and crystals.
- [44] M. V. Jaric, *Introduction to the mathematics of quasicrystals* (Academic Press London, 1989).
- [45] L. S. Levitov, Why only Quadratic Irrationalities are Observed in Quasi-Crystals?, *EPL (Europhysics Letters)* **6**, 517 (1988).
- [46] N. D. Mermin, The space groups of icosahedral quasicrystals and cubic, orthorhombic, monoclinic, and triclinic crystals, *Rev. Mod. Phys.* **64**, 3 (1992).
- [47] D. Smith, J. S. Myers, C. S. Kaplan, and C. Goodman-Strauss, An aperiodic monotile, *Preprint at <https://arxiv.org/abs/2303.10798>* (2023).
- [48] D. Smith, J. S. Myers, C. S. Kaplan, and C. Goodman-Strauss, A chiral aperiodic monotile, *Preprint at <https://arxiv.org/abs/2305.17743>* (2023).
- [49] J. E. S. Socolar, Quasicrystalline structure of the Smith monotile tilings, *Preprint at <https://arxiv.org/abs/2305.01174>* (2023).
- [50] M. Baake, F. Gähler, and L. Sadun, Dynamics and topology of the Hat family of tilings, *Preprint at <https://arxiv.org/abs/2305.05639>* (2023).
- [51] M. Arai, T. Tokihiro, T. Fujiwara, and M. Kohmoto, Strictly localized states on a two-dimensional Penrose lattice, *Phys. Rev. B* **38**, 1621 (1988).
- [52] F. Milde, R. A. Römer, and M. Schreiber, Multifractal analysis of the metal-insulator transition in anisotropic systems, *Phys. Rev. B* **55**, 9463 (1997).
- [53] N. Macé, A. Jagannathan, P. Kalugin, R. Mosseri, and F. Piéchon, Critical eigenstates and their properties in one- and two-dimensional quasicrystals, *Phys. Rev. B* **96**, 045138 (2017).
- [54] V. Goblot, A. Štrkalj, N. Pernet, J. L. Lado, C. Dorow, A. Lemaitre, L. Le Gratiet, A. Harouri, I. Sagnes, S. Ravets, A. Amo, J. Bloch, and O. Zilberberg, Emergence of criticality through a cascade of delocalization transitions in quasiperiodic chains, *Nature Physics* **16**, 832 (2020).
- [55] A. Jagannathan, Closing of gaps and gap labeling and passage from molecular states to critical states in a 2D quasicrystal, *Preprint at <https://arxiv.org/abs/2304.04409>* (2023).
- [56] F. Evers and A. D. Mirlin, Anderson transitions, *Rev. Mod. Phys.* **80**, 1355 (2008).
- [57] F. Flicker, S. H. Simon, and S. A. Parameswaran, Classical dimers on Penrose tilings, *Phys. Rev. X* **10**, 011005 (2020).
- [58] M. O. Oktel, Strictly localized states in the octagonal Ammann-Beenker quasicrystal, *Phys. Rev. B* **104**, 014204 (2021).
- [59] A. Weiße, G. Wellein, A. Alvermann, and H. Fehske, The kernel polynomial method, *Rev. Mod. Phys.* **78**, 275 (2006).
- [60] Q. Marsal, D. Varjas, and A. G. Grushin, Topological Weaire-Thorpe models of amorphous matter, *Proceedings of the National Academy of Sciences* **117**, 30260 (2020).
- [61] Q. Marsal, D. Varjas, and A. G. Grushin, Obstructed insulators and flat bands in topological phase-change materials, *Phys. Rev. B* **107**, 045119 (2023).
- [62] P. Corbae, S. Ciocys, D. Varjas, E. Kennedy, S. Zeltmann, M. Molina-Ruiz, S. M. Griffin, C. Jozwiak,

- Z. Chen, L.-W. Wang, A. M. Minor, M. Scott, A. G. Grushin, A. Lanzara, and F. Hellman, Observation of spin-momentum locked surface states in amorphous Bi₂Se₃, *Nature Materials* **22**, 200 (2023).
- [63] S. T. Ciocys, Q. Marsal, P. Corbae, D. Varjas, E. Kennedy, M. Scott, F. Hellman, A. G. Grushin, and A. Lanzara, Establishing Coherent Momentum-Space Electronic States in Locally Ordered Materials, [Preprint at https://arxiv.org/abs/2302.05945](https://arxiv.org/abs/2302.05945) (2023).
- [64] E. Rotenberg, W. Theis, K. Horn, and P. Gille, Quasicrystalline valence bands in decagonal alnico, *Nature* **406**, 602 (2000).
- [65] E. Rotenberg, W. Theis, and K. Horn, Electronic structure investigations of quasicrystals, *Progress in Surface Science* **75**, 237 (2004).
- [66] V. A. Rogalev, O. Gröning, R. Widmer, J. H. Dil, F. Bisti, L. L. Lev, T. Schmitt, and V. N. Strocov, Fermi states and anisotropy of Brillouin zone scattering in the decagonal Al-Ni-Co quasicrystal, *Nature Communications* **6**, 8607 (2015).
- [67] A. H. Castro Neto, F. Guinea, N. M. R. Peres, K. S. Novoselov, and A. K. Geim, The electronic properties of graphene, *Rev. Mod. Phys.* **81**, 109 (2009).
- [68] B. Sutherland, Localization of electronic wave functions due to local topology, *Phys. Rev. B* **34**, 5208 (1986).
- [69] The Supplemental Material includes a discussion on the spatial structure of zero-modes at zero and π -flux, a discussion on their counting, and tables enumerating them for different quasicrystallites.
- [70] E. Day-Roberts, R. M. Fernandes, and A. Kamenev, Nature of protected zero-energy states in Penrose quasicrystals, *Phys. Rev. B* **102**, 064210 (2020).
- [71] R. Bhola, S. Biswas, M. M. Islam, and K. Damle, Dulmage-mendelsohn percolation: Geometry of maximally packed dimer models and topologically protected zero modes on site-diluted bipartite lattices, *Phys. Rev. X* **12**, 021058 (2022).
- [72] A. Koga and H. Tsunetsugu, Antiferromagnetic order in the Hubbard model on the Penrose lattice, *Phys. Rev. B* **96**, 214402 (2017).
- [73] J. Lloyd, S. Biswas, S. H. Simon, S. A. Parameswaran, and F. Flicker, Statistical mechanics of dimers on quasiperiodic ammann-beenker tilings, *Phys. Rev. B* **106**, 094202 (2022).
- [74] H. Ha and B.-J. Yang, Macroscopically degenerate localized zero-energy states of quasicrystalline bilayer systems in the strong coupling limit, *Phys. Rev. B* **104**, 165112 (2021).
- [75] H. Cohen, *A Course in Computational Algebraic Number Theory* (Springer Verlag, 1993).
- [76] R. Kannan and A. Bachem, Polynomial algorithms for computing the smith and hermite normal forms of an integer matrix, *SIAM Journal on Computing* **8**, 499 (1979).
- [77] R. Ghadimi, T. Sugimoto, and T. Tohyama, Higher-dimensional Hofstadter butterfly on the Penrose lattice, *Phys. Rev. B* **106**, L201113 (2022).
- [78] D. J. Thouless, M. Kohmoto, M. P. Nightingale, and M. den Nijs, Quantized Hall Conductance in a Two-Dimensional Periodic Potential, *Phys. Rev. Lett.* **49**, 405 (1982).
- [79] Q. Niu, D. J. Thouless, and Y.-S. Wu, Quantized Hall conductance as a topological invariant, *Phys. Rev. B* **31**, 3372 (1985).
- [80] R. Bianco and R. Resta, Mapping topological order in coordinate space, *Phys. Rev. B* **84**, 241106 (2011).
- [81] S. Datta, [Quantum Transport: Atom to Transistor](https://doi.org/10.1017/CBO9780511527622) (Cambridge University Press, 2005).
- [82] C. W. Groth, M. Wimmer, A. R. Akhmerov, and X. Waintal, Kwant: a software package for quantum transport, *New Journal of Physics* **16**, 063065 (2014).
- [83] S. J. Ahn, P. Moon, T.-H. Kim, H.-W. Kim, H.-C. Shin, E. H. Kim, H. W. Cha, S.-J. Kahng, P. Kim, M. Koshino, Y.-W. Son, C.-W. Yang, and J. R. Ahn, Dirac electrons in a dodecagonal graphene quasicrystal, *Science* **361**, 782 (2018).
- [84] G. Yu, Z. Wu, Z. Zhan, M. I. Katsnelson, and S. Yuan, Dodecagonal bilayer graphene quasicrystal and its approximants, *npj Computational Materials* **5**, 122 (2019), 1907.08792.
- [85] P. Kot, J. Parnell, S. Habibian, C. Straßer, P. M. Ostrovsky, and C. R. Ast, Band dispersion of graphene with structural defects, *Phys. Rev. B* **101**, 235116 (2020).
- [86] M. A. Bandres, M. C. Rechtsman, and M. Segev, Topological photonic quasicrystals: Fractal topological spectrum and protected transport, *Phys. Rev. X* **6**, 011016 (2016).
- [87] M. Notomi, H. Suzuki, T. Tamamura, and K. Edagawa, Lasing action due to the two-dimensional quasiperiodicity of photonic quasicrystals with a Penrose lattice, *Phys. Rev. Lett.* **92**, 123906 (2004).
- [88] L. Levi, M. Rechtsman, B. Freedman, T. Schwartz, O. Manela, and M. Segev, Disorder-Enhanced Transport in Photonic Quasicrystals, *Science* **332**, 1541 (2011).
- [89] D. Tanese, E. Gurevich, F. Baboux, T. Jacqmin, A. Lemaître, E. Galopin, I. Sagnes, A. Amo, J. Bloch, and E. Akkermans, Fractal energy spectrum of a polariton gas in a Fibonacci quasiperiodic potential, *Phys. Rev. Lett.* **112**, 146404 (2014).
- [90] A. Stegmaier, H. Brand, S. Imhof, A. Fritzsche, T. Helbig, T. Hofmann, I. Boettcher, M. Greiter, C. H. Lee, G. Bahl, A. Szameit, T. Kießling, R. Thomale, and L. K. Upreti, Realizing efficient topological pumping in electrical circuits, [Preprint at https://arxiv.org/abs/2306.15434](https://arxiv.org/abs/2306.15434) (2023).
- [91] P. Vignolo, M. Bellec, J. Böhm, A. Camara, J.-M. Gambaudo, U. Kuhl, and F. Mortessagne, Energy landscape in a Penrose tiling, *Phys. Rev. B* **93**, 075141 (2016).
- [92] Y. Chen, M. Kadic, S. Guenneau, and M. Wegener, Isotropic chiral acoustic phonons in 3D quasicrystalline metamaterials, *Phys. Rev. Lett.* **124**, 235502 (2020).
- [93] Y. Wang and O. Sigmund, Quasiperiodic mechanical metamaterials with extreme isotropic stiffness, *Extreme Mechanics Letters* **34**, 100596 (2020).
- [94] R. Penrose, “The role of aesthetics in pure and applied mathematical research”, *Bulletin of the Institute of Mathematics and its Applications* **10**, 266ff (1974).
- [95] D. Levine and P. J. Steinhardt, Quasicrystals: A new class of ordered structures, *Phys. Rev. Lett.* **53**, 2477 (1984).
- [96] L. A. Bursill and P. Ju Lin, Penrose tiling observed in a quasi-crystal, *Nature* **316**, 50 (1985).
- [97] R. McGrath, J. Ledieu, E. Cox, S. Haq, R. Diehl, C. Jenks, I. Fisher, A. Ross, and T. Lograsso, “Quasicrystal surfaces: potential as templates for molecular adsorption”, *Journal of Alloys and Compounds* **342**, 432 (2002), proceedings from the ‘Quasicrystals 2001’ Conference.

- [98] K. K. Gomes, W. Mar, W. Ko, F. Guinea, and H. C. Manoharan, Designer Dirac fermions and topological phases in molecular graphene, *Nature* **483**, 306 (2012).
- [99] S. N. Kempkes, M. R. Slot, S. E. Freeney, S. J. M. Zevenhuizen, D. Vanmaekelbergh, I. Swart, and C. M. Smith, Design and characterization of electrons in a fractal geometry, *Nature Physics* **15**, 127 (2019).
- [100] S. Nadj-Perge, I. K. Drozdov, B. A. Bernevig, and A. Yazdani, Proposal for realizing Majorana fermions in chains of magnetic atoms on a superconductor, *Phys. Rev. B* **88**, 020407 (2013).
- [101] L. Schneider, P. Beck, J. Neuhaus-Steinmetz, L. Rózsa, T. Posske, J. Wiebe, and R. Wiesendanger, Precursors of Majorana modes and their length-dependent energy oscillations probed at both ends of atomic Shiba chains, *Nature Nanotechnology* **17**, 384 (2022).
- [102] M. O. Soldini, F. Küster, G. Wagner, S. Das, A. Aldarawshah, R. Thomale, S. Lounis, S. S. P. Parkin, P. Sessi, and T. Neupert, Two-dimensional Shiba lattices as a possible platform for crystalline topological superconductivity, *Nature Physics* [10.1038/s41567-023-02104-5](https://doi.org/10.1038/s41567-023-02104-5) (2023).
- [103] E. Babaev, D. Kharzeev, M. Larsson, A. Molochkov, and V. Zhaunerchyk, *Chiral Matter* (WORLD SCIENTIFIC, 2023).
- [104] T. Morimoto and N. Nagaosa, Chiral anomaly and giant magnetochiral anisotropy in noncentrosymmetric weyl semimetals, *Phys. Rev. Lett.* **117**, 146603 (2016).
- [105] J. Ma and D. A. Pesin, Chiral magnetic effect and natural optical activity in metals with or without Weyl points, *Phys. Rev. B* **92**, 235205 (2015).
- [106] S. Zhong, J. E. Moore, and I. Souza, Gyrotropic magnetic effect and the magnetic moment on the Fermi surface, *Phys. Rev. Lett.* **116**, 077201 (2016).
- [107] F. Flicker, F. de Juan, B. Bradlyn, T. Morimoto, M. G. Vergniory, and A. G. Grushin, Chiral optical response of multifold fermions, *Phys. Rev. B* **98**, 155145 (2018).
- [108] Y.-Q. Wang, T. Morimoto, and J. E. Moore, Optical rotation in thin chiral/twisted materials and the gyrotropic magnetic effect, *Phys. Rev. B* **101**, 174419 (2020).
- [109] X. Hu, M. Kargarian, and G. A. Fiete, Topological insulators and fractional quantum Hall effect on the ruby lattice, *Phys. Rev. B* **84**, 155116 (2011).
- [110] Y. Liu, L. F. Santos, and E. Prodan, Topological gaps in quasiperiodic spin chains: A numerical and k-theoretic analysis, *Phys. Rev. B* **105**, 035115 (2022).
- [111] C. Kaplan, *An aperiodic monotile*.

Supplemental Material to: Physical properties of the Hat aperiodic monotile: Graphene-like features, chirality and zero-modes

Justin Schirmann,^{1,*} Selma Franca ,^{1,†} Felix Flicker ,^{2,3,‡} and Adolfo G. Grushin ,^{1,§}

¹Univ. Grenoble Alpes, CNRS, Grenoble INP, Institut Néel, 38000 Grenoble, France

²School of Physics and Astronomy, Cardiff University,
The Parade, Cardiff CF24 3AA, United Kingdom

³School of Physics, H. H. Wills Physics Laboratory,
Tyndall Avenue, Bristol, BS8 1TL, United Kingdom

(Dated: July 31, 2023)

I. FURTHER DETAILS ON ZERO-MODES

A. Zero-modes at zero magnetic field

In the main text we have discussed the conditions that the wave function must satisfy to be a zero-mode at $\phi/\phi_0 = 0$. In Table I we list the number of zero-modes for the different inflations of the primitive metatiles (H0,T0,P0 and F0).

Inflation	H	T	P	F
0	0	0	1	1
1	0	0	0	0
2	8	0	1	1
3	51	8	27	32

Table I. Number of exact zero-modes for each generation of inflation rules in the case of $\phi/\phi_0 = 0$.

For completeness, we comment on the expected robustness of these zero-modes compared to other quasicrystalline zero-modes. The zero-modes found on the Penrose tiling are topologically protected, in the sense that they survive arbitrary changes to the hopping integrals provided these remain nonzero. This is a consequence of Lieb's theorem for bipartite graphs [1], and can be understood in terms of dimer matchings [2–4]. In the Ammann-Beenker tiling the zero-modes are fragile: they receive no such protection, and changing the hoppings breaks the local symmetries of the graph and lifts the degeneracy of these modes [4]. As the Hat tiling is non-bipartite, Lieb's theorem does not apply, and the zero-modes are expected to be fragile.

B. Zero-modes at π -flux

Introducing a π -flux per plaquette, we have observed that the number of modes with energies smaller than 5×10^{-5} matches the number of anti-hats in the Hat quasicrystallites of generations 1, 2 and 3, as shown in Table II.

An exception to this observation are the P and F Hat tilings in generation 0, that consist of the same arrange-

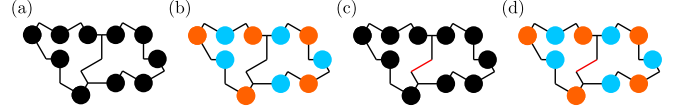


Figure S1. Properties of a zero-mode wave-function Ψ_{zm} in case of the P0 Hat. Panels (a) and (b) show $|\Psi_{zm}|^2$ and Ψ_{zm} , respectively, in real-space for the case of 0-flux. Panels (c) and (d) show $|\Psi_{zm}|^2$ and Ψ_{zm} , respectively, in real-space for the case of π -flux. In all panels, black lines represent positive hoppings and red lines negative hoppings.

ment of hat tiles. For this reason, we discuss only P0 Hat tiling in the following. It has no anti-hats but hosts a single zero-mode. This is surprising since none of the tiles in these Hats have $2m + 2$ vertices, required to host a zero-mode in presence of a π -flux. We observe that these zero-modes are localized at the outer edges of respective systems and their LDOS and Ψ_{zm} is identical to the LDOS and Ψ_{zm} of zero-modes in the case of 0-flux, see Fig. S1. This suggests that zero-modes in both cases (0- and π -flux) fulfill the same set of constraints. We can understand this by noting that it is possible to find a gauge in which the π -flux is implemented via a single, negative hopping amplitude between vertices that are shared between hats that form P0 Hat tiling. One possible such configuration of hopping amplitudes is shown in Figs. S1 (c-d). Therefore, the hopping amplitudes between vertices belonging to the boundaries of the sample can always be considered identical. Since there are $4m$ ($m = 5$) such vertices, the system can host a zero-mode under the same conditions it hosts a zero-mode in case of 0-flux.

Inflation	H		T		P		F	
	AH	ZM	AH	ZM	AH	ZM	AH	ZM
0	1	1	0	0	0	1	0	1
1	3	3	1	1	2	2	2	2
2	22	22	3	3	12	12	14	14
3	147	147	8	8	84	84	98	98

Table II. Number of anti-hats (AH) and exact zero-modes (ZM) for each generation of inflation rules for magnetic flux $\phi/\phi_0 = 1/2$.

Another exception we have observed is in quasicrystallites with anti-hats at the boundary (which are therefore not generated by inflation). In these cases there are fewer zero-modes than anti-hats. In such cases the environment around the boundary anti-hats can frustrate the zero-mode.

II. ZERO-MODE REAL-SPACE STRUCTURE AND COUNTING

The electronic zero-modes in the tight-binding model are solutions to the equation

$$H |\psi_{zm}\rangle = 0, \quad (1)$$

where H is the tight-binding Hamiltonian described by Eq. (1) in the main text. This Hamiltonian defines the adjacency matrix of the undirected graph formed by the union of hats. The number of zero-modes is then equal to the rank deficiency of H (the number of columns minus the number of linearly independent columns).

In the 0-flux case it is possible to find a basis for the (un-normalized) zero-modes in which the amplitude on each vertex is an integer, and many vertices have zero amplitude. These are a generalisation of the strictly localised zero-modes of Sutherland [5]. To illustrate this, we study several small quasicrystallites shown in Fig. S2. If a quasicrystallite system supports a zero-mode, we then plot the corresponding amplitudes of $|\psi_{zm}\rangle$ in real-space. From Figs. S2(a-b), we see that whenever the graph contains a cycle of length $4m$, with m integer, the amplitudes around the cycle can be taken to be the repeated sequence $\{0, 1, 0, -1\}^m$ and a system supports a zero-mode. As illustrated in Figs. S2(c-e), these zero-modes are preserved once additional hats are added to the quasicrystallite, provided that vertices from the rest of the graph connect only to cycle vertices of zero amplitude. This implies that the remaining graph needs to connect to vertices separated by even distances along the cycle, as these vertices can be chosen to have weight zero without implying nonzero weights off the cycle.

There may also be other integer-amplitude zero-modes

not of the form just stated, see Figs. S2(f-h). This is because, in general, it is possible to find integer-amplitude zero-modes by writing H in its Hermite normal form N :

$$N = UH, \quad (2)$$

where N contains one column of zeroes for each zero-mode (there are various further restrictions on the form of N which render the decomposition unique) [6]. The integer unimodular matrix U can be calculated efficiently using Gaussian elimination. For each zero column of N , the corresponding column in U contains the amplitudes of the wave-function on each graph vertex. For example, the graph of P2 metatyle shown in Fig. S2(h) supports a zero-mode with wave-function amplitudes that range in magnitude from 0 to 6. Since there is only one mode, there is no possibility of decomposing it into a different basis with smaller amplitudes.

* justin.schirmann@neel.cnrs.fr;

* These two authors contributed equally

† selma.franca@neel.cnrs.fr;

These two authors contributed equally

‡ flicker@cardiff.ac.uk

§ adolfo.grushin@neel.cnrs.fr

- [1] E. H. Lieb, Two theorems on the Hubbard model, *Phys. Rev. Lett.* **62**, 1201 (1989).
- [2] F. Flicker, S. H. Simon, and S. A. Parameswaran, Classical dimers on Penrose tilings, *Phys. Rev. X* **10**, 011005 (2020).
- [3] R. Bhola, S. Biswas, M. M. Islam, and K. Damle, Dulmage-mendelsohn percolation: Geometry of maximally packed dimer models and topologically protected zero modes on site-diluted bipartite lattices, *Phys. Rev. X* **12**, 021058 (2022).
- [4] J. Lloyd, S. Biswas, S. H. Simon, S. A. Parameswaran, and F. Flicker, Statistical mechanics of dimers on quasiperiodic ammann-beenker tilings, *Phys. Rev. B* **106**, 094202 (2022).
- [5] B. Sutherland, Localization of electronic wave functions due to local topology, *Phys. Rev. B* **34**, 5208 (1986).
- [6] R. Kannan and A. Bachem, Polynomial algorithms for computing the smith and hermite normal forms of an integer matrix, *SIAM Journal on Computing* **8**, 499 (1979).

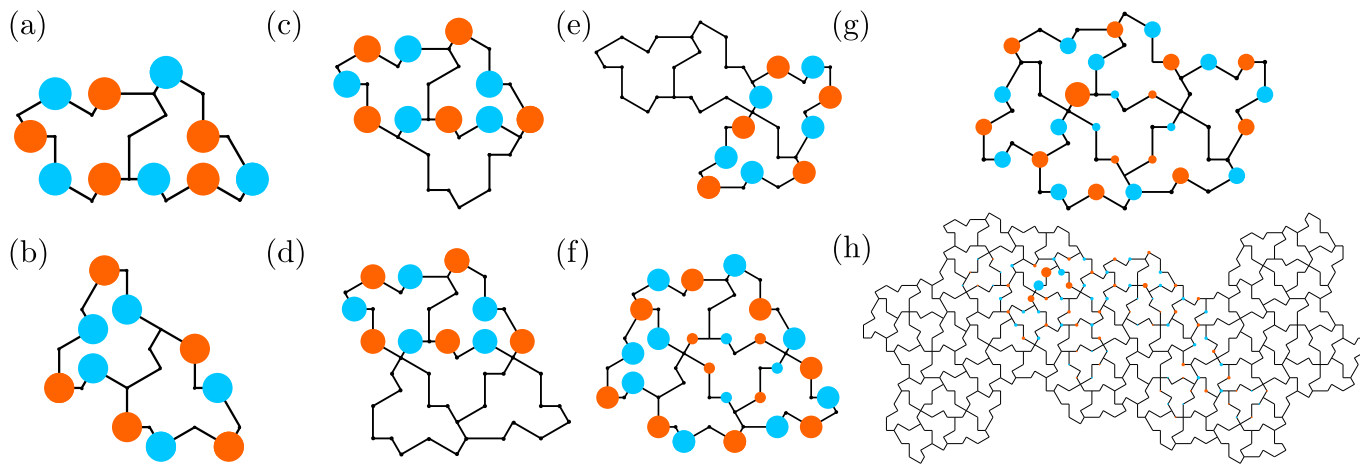


Figure S2. Amplitudes of the zero-mode wavefunction $|\psi_{zm}\rangle$ for different quasicrystallites, including the P2 Hat tiling in panel (h).